THE JOURNAL OF PHYSICAL CHEMISTRY B

ARTICLE

pubs.acs.org/JPCB

Molecular Mechanism of the Effects of Salt and pH on the Affinity between Protein A and Human Immunoglobulin G1 Revealed by Molecular Simulations

Bo Huang, Fu-Feng Liu,* Xiao-Yan Dong, and Yan Sun*

Department of Biological Engineering and Key Laboratory of Systems Bioengineering of the Ministry of Education, School of Chemical Engineering and Technology, Tianjin University, Tianjin 300072, China

Supporting Information

ABSTRACT: Protein A from the bacterium *Staphylococcus aureus* (SpA) has been widely used as an affinity ligand for purification of immunoglobulin G (IgG). The affinity between SpA and IgG is affected differently by salt and pH, but their molecular mechanisms still remain unclear. In this work, molecular dynamics simulations and molecular mechanics Poisson−Boltzmann surface area analysis were performed to investigate the salt (NaCl) and pH effects on the affinity between SpA and human IgG1 (hIgG1). It is found that salt and pH affect the interactions of the hot spots of SpA by different mechanisms. In the salt solution, the compensations between helices I and II of SpA as well as between the nonpolar and electrostatic energies make the binding free energy independent of salt concentration. At pH 3.0, the unfavorable electrostatic interactions increase greatly and become the driving force for dissociation of the SpA−hIgG1 complex. They mainly come from the strong electrostatic repulsions between positively charged residues (H137, R146, and K154) of SpA and the positively charged residues of hIgG1. It is considered to be the molecular basis for hIgG1 elution from SpA-based affinity adsorbents at pH 3.0. The dissociation mechanism is then used to refine the binding model of SpA to hIgG1. The model is expected to help design high-affinity peptide ligands of IgG.

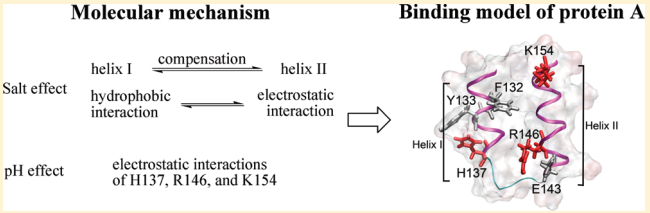

1. INTRODUCTION

Immunoglobulins (Ig) are globular proteins used by the immune system to identify and neutralize antigens. In addition, IgG is the most important family of Igs with many applications in therapeutics, immunodiagnostics, and immunochromatography on the basis of the high affinity between IgG and specific antigens.[1] These applications generally require highly purified IgG. Due to the presence of a huge number of different compounds in the production media, IgG used for medical applications has been thoroughly purified using a combination of various methods, such as precipitation and chromatographic techniques including ion exchange, hydrophobic interaction, and affinity chromatographies.[2−4] Among them, affinity chromatography plays an important role in the industrial-scale purification of IgG.[5] This technique requires an appropriate ligand, which is able to bind IgG with high yield and selectivity.

Thus far, protein A from the bacterium *Staphylococcus aureus* (SpA) is the most popular affinity ligand for IgG[6] due to its specific interactions with the consensus binding site of IgG.[7] In addition, SpA has been used as the industrial standard for IgG purification. Nevertheless, protein A affinity chromatography faces the following two critical challenges. First, IgG is usually eluted under the condition of pH 3.0 due to its high affinity with SpA.[8] The harsh elution and the following regeneration conditions tend to make the highly costly SpA ligand lose its activity.[9] Second, the leaching of SpA may cause harmful immunogenic responses in humans.[10] To address these issues and to design the new peptide ligand, it is necessary to understand the molecular mechanism of the affinity interactions between SpA and IgG.

To date, some research has been carried out to investigate the interactions between IgG and SpA. SpA consists of five repeating Fc-binding domains, each of which is a three-helix bundle.[11] Among the three antiparallel helices, only two of them are involved in the protein−protein binding interface, which is located in the hinge region that connects the second and third constant domains (CH2 and CH3) of the Fc fragment. The binding site of the Fc fragment is distinguished, and the nature of the interactions between SpA and IgG has been characterized.[8,12,13] In addition to experimental research, some computational simulations have been performed to provide more molecular details of the SpA-IgG complexes. For example, the binding free energies between IgG and SpA[14] or SpA-mimic ligands[15,16] were calculated by molecular dynamics (MD) simulations. Our previous research shows that the binding is regulated by six residues of SpA (F132, Y133, H137, E143, R146, and K154), which are defined as the hot spots of SpA.[17] In addition, then the binding motif of SpA is constructed, which would provide guidance to design novel high-affinity ligands of IgG.

As we know, ideal ligands suitable for affinity chromatography should have high affinity, high binding capacity, and selectivity

Received: June 20, 2011
Revised: December 2, 2011
Published: December 04, 2011

Table 1. Properties of Molecular Systems Used in MD Simulations

system	N_{Cl^-}	N_{Na^+}	N_{water}	simulation length/ns
pH 7.0, water	0	1	9197	50
pH7.0, 0.5 mol/L NaCl	81	82	8567	50
pH7.0, 1.0 mol/L NaCl	163	164	8403	50
pH7.0, 2.0 mol/L NaCl	326	327	8077	50
pH 3.0, water	34	0	9149	70

for the target. Moreover, elution of adsorbed proteins should be gentle and controlled.[18] Many studies have shown that the adsorbed IgG is eluted off the SpA affinity adsorbent under harsh elution condition (pH 3.0) rather than NaCl solutions.[19,20] Hence, in order to improve the performance of SpA ligand and design new SpA-mimic affinity ligands, the first concern is to understand the interactions between SpA and IgG not only at the binding condition but also at the dissociation condition.

Although the binding molecular mechanism of the SpA−IgG complex has been revealed by experimental and simulation studies, the molecular mechanism at different elution conditions is not yet clear. Herein, we employed MD simulations and the molecular mechanics Poisson−Boltzmann surface area (MM/PBSA) method to investigate the effect of pH and salt (NaCl) on the affinity interactions between SpA and human Immunoglobulin G1 (hIgG1), since it is difficult to elucidate the molecular details by the available experimental approaches. First, the binding free energies were calculated using the MM/PBSA method. Then, the free energy decomposition was used to analyze the energy contributions of the residues located in the binding site. Thereafter, the molecular basis of SpA's affinity for hIgG1 at different conditions was discussed by comparing the effects of salt and pH on the roles of the hot spots. Finally, these molecular mechanisms were used to refine the simplified binding model of SpA. Such information not only provides fundamental understanding of the affinity between SpA and hIgG1 but also offers substantial information to the rational design of novel affinity ligands.

2. METHODS

Molecular Systems. Five systems with different concentrations of NaCl or at different pH were built for MD simulations (Table 1). Each molecular system contained a single heavy chain of the Fc fragment of hIgG1 and the B domain of SpA (Figure S1A, Supporting Information). The coordinates of the proteins were obtained from the X-ray structure in Protein Data Bank (PDB ID 1FC2).[6] The complex was solvated in a box (85 × 54 × 72 Å) using TIP3P water. The different pH was mimicked by different protonation states of residues.[21,22] For all simulations at pH 7.0 and 3.0, the N termini and basic residues (Lys and Arg) were protonated and the C termini were deprotonated. The acidic residues (Asp and Glu) were deprotonated at pH 3.0 and protonated at pH 7.0. His residues were protonated at pH 3.0 and kept neutral at pH 7.0. Na^+ and Cl^- as salt ions were added according to the corresponding concentration of NaCl and the charges of proteins (Table 1).

Molecular Dynamics Simulations. All MD simulations were performed using NAMD[23] with the all-atom CHARMM27 force field.[24] The temperature was set to 298 K and kept constant during the simulation process using a Langevin thermostat with a damping coefficient of 0.5 ps^{-1} for temperature control.[25] After minimization, the system was equilibrated for 200 ps. Then the production phase of the simulation was carried out in the isothermal−isobaric ensemble. The pressure was kept at 1.0 atm using a Nosé−Hoover langevin piston[26] with a piston period of 200 fs and a decay time of 100 fs. Periodic boundary condition was used for all MD simulations. Nonbonded interactions were cut off at 12 Å, with shifting throughout the interaction range for electrostatic interactions and beginning at 9 Å for vdW interactions to implement a smooth cutoff. In addition, the particle mesh Ewald method[27] was used to handle the long-range electrostatic interactions. The SHAKE method[28] was applied to restraining covalent bonds involving all hydrogen atoms, which allowed use of a time step of 2 fs. A distance restraint was imposed on the two terminal residues of hIgG1 to avoid the relative bending of the CH2 and CH3 domains for the system only contained a single chain of hIgG1. Two hundred fifty conformations of each complex were extracted from the last 10 ns of the production phase at an interval of 40 ps. Data were used for further analysis described below to calculate free energies. The free energy data calculated from the 250 conformations were averaged and are plotted in the figures (Figures 2−6 and 8) with error bars representing the standard deviations.

Binding Free Energy Calculation. The MM/PBSA[29,30] method was used to calculate the binding free energy (ΔG_{bind}) for the SpA−hIgG1 complex by the CHARMM[31] program with the all-atom CHARMM27 force field. The binding free energy was estimated as the sum of the gas-phase energy (ΔG_{gas}) and the solvation energy (ΔG_{sol}) according to

$$\Delta G_{bind} = \langle \Delta G_{gas} \rangle + \langle \Delta G_{sol} \rangle \quad (1)$$

The brackets, ⟨...⟩, indicate an average of an energy term along the MD simulation trajectory. G_{gas} contains an intermolecular electrostatic term (G_{elec}), a van der Waals (vdW) term (G_{vdw}), and an internal energy term (G_{inter}). In this study, "the same trajectory method"[32] was used in all analyses. Thus, the internal energy term (ΔG_{inter}) is zero, and ΔG_{gas} is the sum of ΔG_{elec} and ΔG_{vdw}.

$$\Delta G_{gas} = \Delta G_{elec} + \Delta G_{vdw} \quad (2)$$

The solvation energy is divided into the electrostatic solvation energy (G_{PB}) and the nonpolar solvation energy (G_{np})

$$G_{sol} = G_{PB} + G_{np} \quad (3)$$

G_{PB} was calculated by solving the linear Poisson−Boltzmann (PB) equation using the PBEQ module of the CHARMM program. The solute and solvent dielectric constants were set to 1 and 80, respectively. G_{np}, which could be considered as the sum of a solvent−solvent cavity term and a solute−solvent vdW term, was calculated according to

$$Gnp = \gamma \times SASA + b \quad (4)$$

The constants γ and b were set to 0.00542 kcal/(mol·Å^2) and 0.92 kcal/mol, respectively.[33] The solvent-accessible surface area (SASA) was calculated using a water probe radius of 1.4 Å.

Free Energy Decomposition. The free energy contribution of each residue can be divided into electrostatic (G_{PBelec}) and nonpolar ($G_{nonpolar}$) components according to eq 5. The electrostatic component of the free energy (G_{PBelec}) is defined as the sum of the electrostatic solvation energy (G_{PB}) and the intermolecular electrostatic energy (G_{elec}) (eq 6);[34−38] the nonpolar

energy of each residue ($G_{nonpolar}$) includes the van der Waals interaction energy (G_{vdw}) and nonpolar solvation term (G_{np}) (eq 7).[37−39]

$$G_{residue} = G_{PBelec} + G_{nonpolar} \quad (5)$$

$$G_{PBelec} = G_{PB} + G_{elec} \quad (6)$$

$$G_{nonpolar} = G_{vdw} + G_{np} \quad (7)$$

The electrostatic contribution was decomposed by residues according to eq 8.[40] The linear PB equation allowed decomposition of the electrostatic solvation energy, since the electrostatic potential at point i (ϕ_i) can be calculated as the sum of the potentials created by other individual charges.

$$\Delta G^{j}_{elec} = \sum_{i \in \text{complex}} \frac{1}{2} q_i \phi_i^{j \in \text{complex}} - \left[\sum_{i \in \text{hIgG1}} \frac{1}{2} q_i \phi_i^{j \in \text{hIgG1}} + \sum_{i \in \text{SpA}} \frac{1}{2} q_i \phi_i^{j \in \text{SpA}} \right] \quad (8)$$

The vdW energy (G_{vdw}) of each residue of SpA was estimated as one-half of the vdW energy between itself and hIgG1 and vice versa for hIgG1. The nonpolar solvation energy (G_{np}) of each residue was proportional to the loss in SASA based on eq 4.

3. RESULTS AND DISCUSSION

The SpA model studied here is the B domain of SpA, which ranges from F124 to A167 in sequence and consists of three α-helices connected by two irregular coils. For clarity, the helix from K126 to H137 and the helix from E144 to D155 are labeled as helix I and helix II, respectively (Figure S1B, Supporting Information). Since neither the coil from D156 to Q159 nor the third helix from S160 to A167 interacts with hIgG1,[17] only the helices I and II with the random coil (L138 to E143) connecting them are investigated in the following sections.

The extensive conformational sampling required by the MM/PBSA calculation is achieved by MD simulations. The root-mean-square deviation (rmsd) of SpA from the initial X-ray structure and the intermolecular potential energy are shown in Figures S2 and S3, Supporting Information, respectively. The rmsd profiles of SpA in water and different NaCl solutions became quite stable after the initial 20 ns (Figure S2, Supporting Information), while the intermolecular potential energy converged slower than the rmsd and reached a plateau after 30 ns (Figure S3, Supporting Information). Taking into account the relatively low resolution of the crystal structure of SpA (2.6−3.3 Å), we conclude that no significant structural shift from the X-ray structure occurred during the MD simulations. In other words, the SpA−hIgG1 complex remains a metastable or a kinetically trapped state. Therefore, 250 conformations of the complex used for the MM/PBSA analysis were extracted from 40 to 50 ns at an interval of 40 ps. For the SpA−hIgG1 complex at pH 3.0, the rmsd profile is not converged and the intermolecular potential energy is above 1400 kcal/mol (Figures S2 and S3, Supporting Information). It means that the complex is unstable at pH 3.0. Thus, the MD simulation is extended to 70 ns to observe the tendency of dissociation. Finally, 250 conformations extracted from the trajectory ranging from 60 to 70 ns were used for the MM/PBSA analysis.

Table 2. Fraction of the Correct Residues in the Interface of Proteins in Different NaCl Solutions

	F/R	
system	hIgG1	SpA
pH 7.0, 0.5 mol/L NaCl	0.81 (0.06)	0.85 (0.04)
pH 7.0, 1.0 mol/L NaCl	0.85 (0.04)	0.91 (0.04)
pH 7.0, 2.0 mol/L NaCl	0.87 (0.05)	0.96 (0.05)

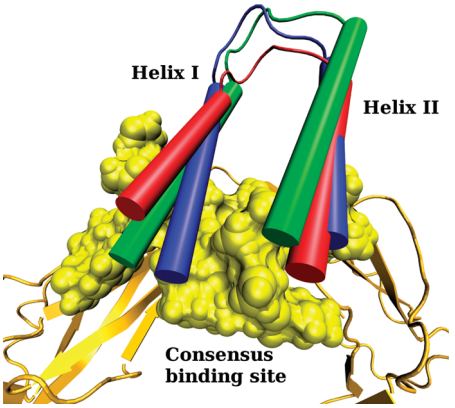

Figure 1. Conformations of SpA binding to hIgG1 in NaCl solutions with different concentrations. The whole hIgG1 is shown in the yellow cartoon model, and its consensus binding site is shown in the yellow surface model. Only the binding parts of SpA are displayed in the cartoon model. The conformation of SpA is colored in blue in 0.5 mol/L NaCl, red in 1.0 mol/L NaCl, and green in 2.0 mol/L NaCl.

3.1. Salt Effect on the Affinity between SpA and hIgG1.

The average rmsd values of SpA in NaCl solutions stabilized in the range of 2.6−3.3 Å, which are similar to that of SpA in water (2.7 Å). It indicates that the salt almost does not affect the conformation of SpA−hIgG1 complex in NaCl solutions ranging from 0 to 2.0 mol/L. The binding interfaces of the complex are further examined in more detail using the fraction of the correct residues in the interface (F/R). F/R is calculated as the number of correct residues in the interface divided by the number of total residues in the interface. The residues in the interface are defined using the cutoff distance between the partner protein of 5 Å.[41] In addition, the correct residues are defined as the residues within the interface using the structure of the SpA−hIgG1 complex in water. The values of F/R of SpA are between 85% and 96% in all of the NaCl solutions (Table 2). It indicates that SpA always binds hIgG1 by helices I and II. In addition, the values of F/R of hIgG1 range from 81% to 87%, which are slightly lower than those of SpA. It means that SpA moves a little and the binding conformation of hIgG1 is slightly different from that in water, as shown in Figure 1.

The MM/PBSA method based on MD simulations was used to calculate the binding free energy (ΔG_{bind}) of the SpA−hIgG1 complex. It was often found that MM/PBSA analyses exaggerate the absolute value of binding free energies.[42−44] There are several sources of errors in the MM/PBSA, including force field, MD sampling, solvation free energy calculated by PBSA, and the low prediction accuracy of the entropic contribution.[45] For the SpA−hIgG1complex in different solutions, entropy contributions arising from the changes in the degrees of freedom

Table 3. Binding Free Energies of the SpA−hIgG1 Complex in Different Solutions (units kcal/mol)

energy[a]	pH 7.0, water	pH 7.0, 0.5 mol/L NaCl	pH 7.0, 1.0 mol/L NaCl	pH 7.0, 2.0 mol/L NaCl	pH 3.0 water
ΔG_{vdw}	−53.0(4)	−48.3(4)	−46.1(5)	−56.0(4)	−40.9(4)
ΔG_{np}	−6.8(0)	−6.7(0)	−7.3(0)	−7.3(0)	−6.8(0)
ΔG_{elec}	−143.3(20)	−123.0(36)	−169.0(22)	−80.9(22)	1497.6(41)
ΔG_{PB}	166.0(17)	139.5(32)	186.2(21)	104.8(19)	−1438(37)
$\Delta G_{nonpolar}$	−59.8(5)	−55.0(4)	−53.4(5)	−63.3(4)	−47.7(5)
ΔG_{PBelec}	22.7(9)	16.5(10)	17.2(9)	23.9(9)	59.6(13)
ΔG_{bind}	−37.1(8)	−38.5(9)	−36.2(10)	−39.4(8)	11.9(11)

[a] ΔG_{np}: nonpolar solvation energy based on the PBSA method. ΔG_{elec}: intermolecular electrostatic energy. ΔG_{PB}: electrostatic solvation energy based on the PBSA method. $\Delta G_{nonpolar}$: nonpolar energy of the SpA−hIgG1 complex. $\Delta G_{nonpolar} = \Delta G_{vdw} + \Delta G_{np}$. ΔG_{PBelec}: electrostatic interaction energy of the SpA−hIgG1 complex. $\Delta G_{PBelec} = \Delta G_{PB} + \Delta G_{elec}$. ΔG_{bind}: binding free energy of the SpA−hIgG1 complex. $\Delta G_{bind} = \Delta G_{nonpolar} + \Delta G_{PBelec}$.

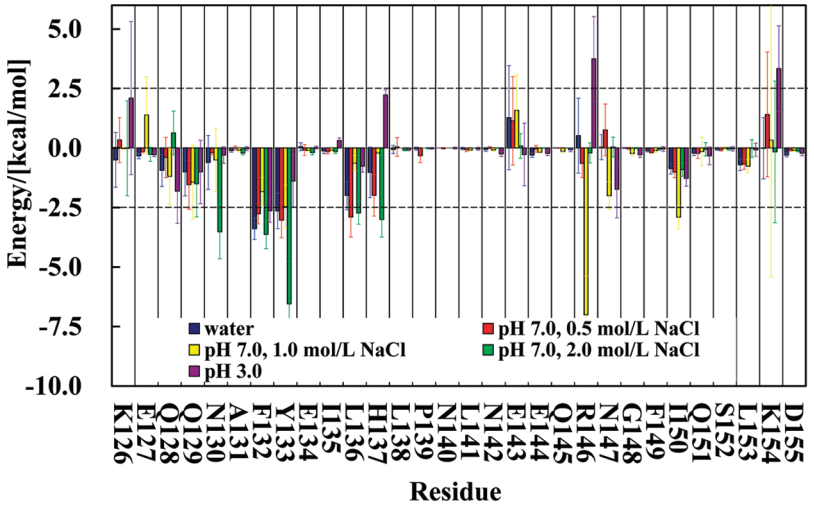

Figure 2. Binding free energy contribution of each residue of SpA in different solutions.

(translational, rotational, and vibrational) of these proteins are very similar and the entropy change is negligible as compared to ΔG_{bind}.[46−48] Therefore, the binding free energy reported here is the relative binding free energy, which neglects the entropy of the proteins. In addition, many studies have proven that the relative binding free energy calculated by MM/PBSA coupled with MD simulations were able to reproduce the trend of affinities of the protein−protein and protein−ligand complexes.[34,49,50] This study aims at shedding some light on how ionic strength and pH impact the association between protein A and IgG. Therefore, the relative binding free energy from the MM/PBSA based on MD simulations would benefit to understand the issue.

Table 3 lists the binding free energies of the SpA−hIgG1 complex in different NaCl solutions calculated by the MM/PBSA method. The calculated binding free energies of the SpA−hIgG1 complexes in different NaCl solutions are from about −36.2 to −39.4 kcal/mol, which are close to that in water (−37.1 kcal/mol), that is, the total binding free energy is affected a little by NaCl. It is in line with the experimental observation that the adsorbed hIgG1 could not be eluted effectively off the SpA affinity adsorbent by NaCl solutions.[51]

To identify the molecular mechanism of the salt effect on the affinity between SpA and hIgG1, the binding free energy was divided into the nonpolar and electrostatic energies. By comparing the energy terms listed in Table 3, it is found that the nonpolar energies ($\Delta G_{nonpolar}$) in NaCl solutions are in the range from −53.4 to −63.3 kcal/mol while the electrostatic energies (G_{PBelec}) play an opposite role (16.5−23.9 kcal/mol). It is noted that the unfavorable electrostatic energies are the consequence of the insufficient compensation between the favorable intermolecular electrostatic energies (ΔG_{elec}) and the larger unfavorable electrostatic solvation effect (ΔG_{PB}). Therefore, salt does not change the types of interactions between SpA and hIgG1 and the nonpolar interactions are also the main driving force for the binding in NaCl solutions.

The energy results in Table 3 show that the nonpolar and electrostatic energies change in the opposite directions. For example, the nonpolar contributions in 0.5 and 1.0 mol/L NaCl are larger than that in water, while the electrostatic contributions are smaller than that in water (Table 3). In 2.0 mol/L NaCl, however, the nonpolar energy is 3.5 kcal/mol lower than that in water, whereas the electrostatic energy is 1.2 kcal/mol higher than that in water (Table 3). Hence, the binding free energy is essentially unchanged by salt. Therefore, the counteraction between the nonpolar and electrostatic interactions makes the total binding free energy insensitive to salt concentration.

Although the binding pattern of the SpA−hIgG1 complex is not changed in salt solutions, the local binding conformations of some residues are affected greatly. As shown by the F/R data in

dx.doi.org/10.1021/jp205770p | J. Phys. Chem. B 2012, 116, 424–433

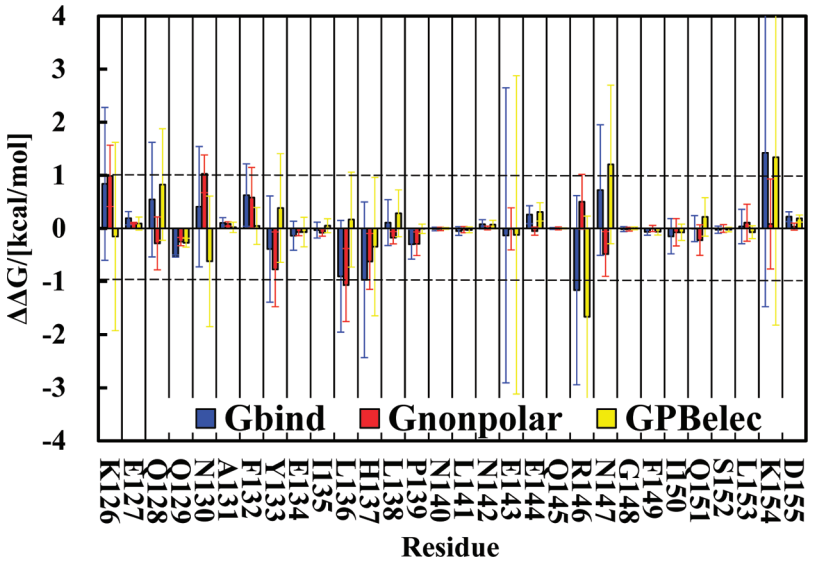

Figure 3. Per-residue decomposition of the binding free energy change ($\Delta\Delta G$) of SpA in 0.5 mol/L NaCl. $\Delta\Delta G = \Delta G(\text{salt}) - \Delta G(\text{water})$.

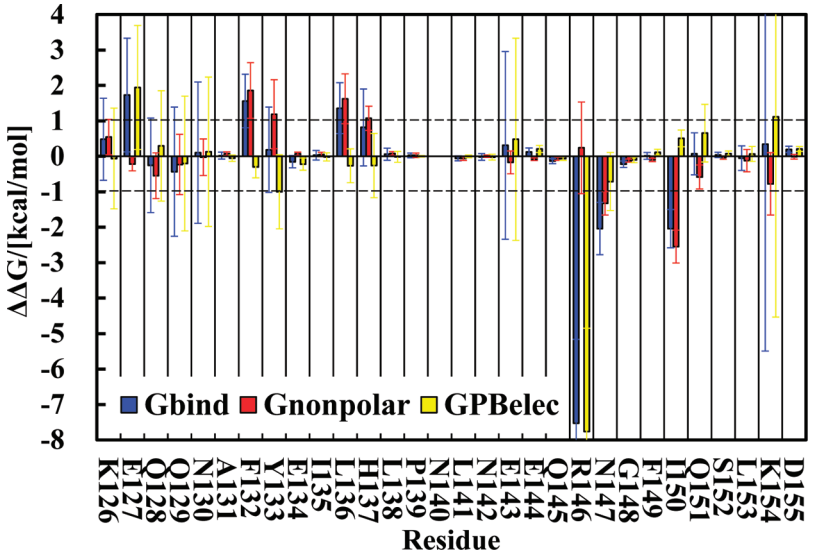

Figure 4. Per-residue decomposition of the binding free energy change ($\Delta\Delta G$) of SpA in 1.0 mol/L NaCl. $\Delta\Delta G = \Delta G(\text{salt}) - \Delta G(\text{water})$.

Table 2 and the conformations in Figure 1, the binding conformations in NaCl solution are slightly different from that in water. Nevertheless, the slight change of binding conformation affects the interactions of the important residues of SpA. Generally, salt has specific and nonspecific influences on the protein−protein association. The specific influence refers to the case that ions stabilize the complex by high-affinity binding to specific sites.[52,53] Besides the specific influence, bulk ionic strength screens the coulomb interactions between charges and the solvation effect of electrostatic residues.[54] In addition, the Hofmeister effect of salt can strengthen the nonpolar interactions by increasing the surface tension of the solvent.[55,56] For the systems studied here, the ions did not participate in the association between SpA and hIgG1 directly, which means NaCl has no specific influence on the binding. However, the nonspecific influence of NaCl affected the contributions of some key residues by changing the ionic strength significantly, which led to the change of the local binding conformation. Since the nonspecific influence of NaCl relates to the nonuniform charge distribution of proteins,[57] it can increase the contributions of some residues and decrease those of some other residues.

To investigate the salt effect on the contributions of the residues, dissection of the binding free energies into per-residue contributions was discussed corresponding to the concentrations of NaCl. The criterion of ±2.5 kcal/mol used in previous work is also employed to identify the important residues having large free energy contributions.[17] As shown in Figure 2, most of the residues of SpA have minimal contributions which are not affected by NaCl solutions. Only eight residues make great contributions, namely, N130, F132, Y133, L136, H137, R146, I150, and K154. In addition, the contributions of these residues are related to the concentrations of NaCl. It is noted that most of these residues are identified as the hot spots of SpA, including F132, Y133, H137, R146, and K154.[14,17] In addition, the other three residues (N130,

L136, and I150) locate around the hot spots. Thus, the affinity of the SpA−hIgG1 complex is dominantly regulated by the hot spots. In order to explain the molecular basis of the salt tolerance, the effect of the concentration of NaCl on the hot spots of SpA is discussed in detail.

0.5 mol/L NaCl. The change of the binding free energy contribution ($\Delta\Delta G$) is introduced to clarify the effect of the salt on the affinity between SpA and hIgG1. It was calculated according to

$$\Delta\Delta G = \Delta G(\text{salt}) - \Delta G(\text{water}) \quad (9)$$

Herein, the criterion of ±1.0 kcal/mol is employed to identify the important residues having a significant change of the free energy contributions. Figure 3 shows the per-residue decomposition results of $\Delta\Delta G$ in 0.5 mol/L NaCl. It is found that only three hot spots (H137, R146, and K154) have significant changes of the free energy contributions, while the other residues of SpA have slight changes in 0.5 mol/L NaCl. From Figure 2, it is shown that the affinity between SpA and hIgG1 in 0.5 mol/L NaCl is also dominated by all of the hot spots of SpA, and only the three hot spots are affected greatly by the salt.

From our previous work, helix I of SpA binds hIgG1 through nonpolar interactions in water while helix II mainly provides electrostatic interactions to regulate the selectivity to different Igs.[17] The residues L136 and H137 of helix I interact with hIgG1 by the nonpolar interactions, which are strengthened in 0.5 mol/L NaCl (Figure 3). The salt also has a favorable effect on the nonpolar contribution of Y133, even though the effect is below the criterion. However, the salt has an unfavorable effect on the nonpolar contributions of K126 and N130, since the residues bind the area nearby the hydrophobic pocket of hIgG1. The opposite responses of those hot spots in 0.5 mol/L NaCl give rise to the small change of the total nonpolar energy. A similar situation also happened to the electrostatic interactions of helix II. For example, R146 and K154 interact with hIgG1 mainly by electrostatic interactions. The electrostatic interactions provided by R146 are strengthened in 0.5 mol/L NaCl. On the contrary, the electrostatic interactions of K154 are weakened by the salt. In addition, the salt is also unfavorable to the electrostatic contribution of N147. Hence, the minor effect of 0.5 mol/L NaCl is caused by the balances among the free energy contributions of important residues of each helix. In addition, it is noted that $\Delta\Delta G_{bind}$ of the other three hot spots of SpA (F132, Y133, and E143) are small. This indicates that the important interactions involving these residues are affected slightly in 0.5 mol/L NaCl.

1.0 mol/L NaCl. As shown in Figure 4, the values of $\Delta\Delta G_{nonpolar}$ of many residues of helix I are positive, including F132, Y133, L136, and H137. It indicates that nonpolar interactions of these residues are reduced greatly in 1.0 mol/L NaCl. In addition, the positive $\Delta\Delta G_{PBelec}$ of E127 means that its electrostatic

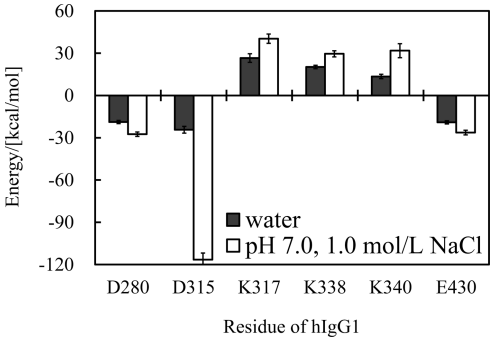

Figure 5. Potential energies between R146 of SpA and the charged residues of hIgG1 in water and 1.0 mol/L NaCl.

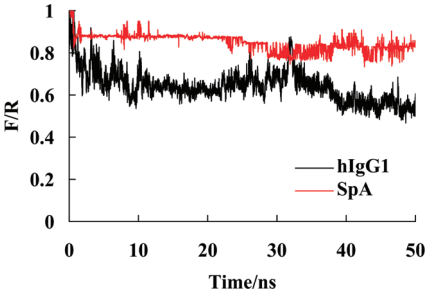

Figure 7. Fraction of the residues in the interface (F/R) of the SpA−hIgG1 complex at pH 3.0.

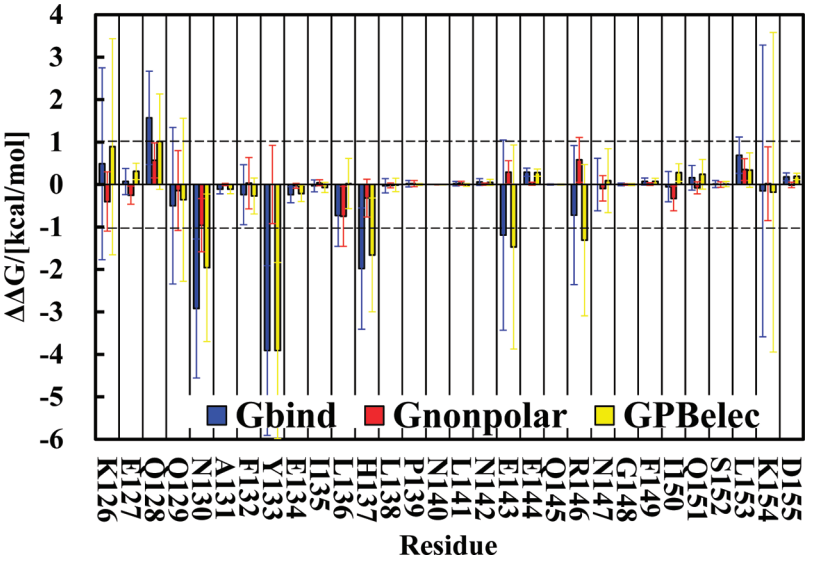

Figure 6. Per-residue decomposition of the binding free energy change ($\Delta\Delta G$) of SpA in 2.0 mol/L NaCl. $\Delta\Delta G = \Delta G(\text{salt}) - \Delta G(\text{water})$.

dx.doi.org/10.1021/jp205770p |*J. Phys. Chem. B* 2012, 116, 424–433

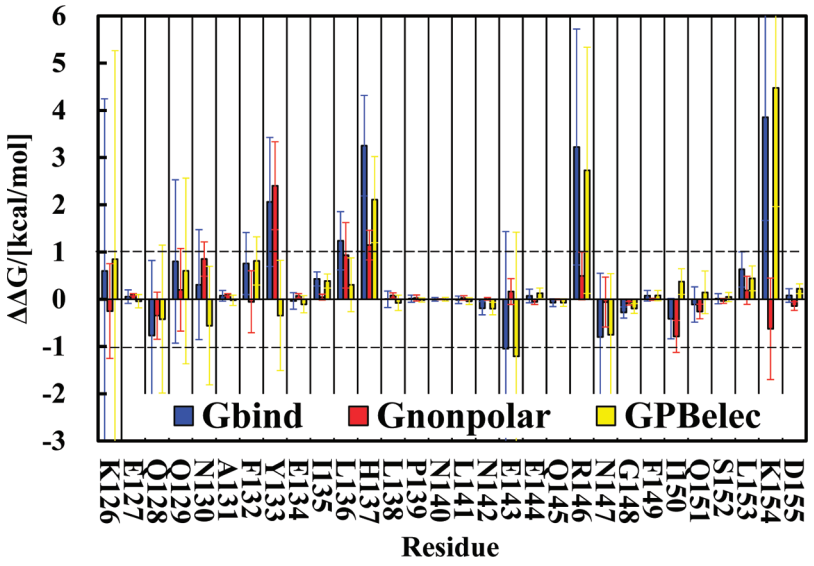

Figure 8. Per-residue decomposition of the binding free energy change ($\Delta\Delta G$) of SpA at pH 3.0. $\Delta\Delta G = \Delta G$(pH 3.0) $- \Delta G$(pH 7.0).

interactions are also weakened in 1.0 mol/L NaCl. It is further validated by the snapshot of helix I of SpA (Figure 1) that helix I slid slightly away from the binding site. Thus, the interactions between helix I and hIgG1 are reduced greatly in 1.0 mol/L NaCl.

Contrary to helix I, the interactions between helix II and hIgG1 are enhanced in 1.0 mol/L NaCl, especially for their electrostatic interactions. The favorable energy mainly originates from the electrostatic contribution of residues R146 and N147 (Figure 4). In particular, $\Delta\Delta G_{PBelec}$ of residue R146 is as low as −7.8 kcal/mol. The positively charged residue R146 interacts with six charged residues of hIgG1, including D280, D315, K317, K338, K340, and E430 (Figure 5). In 1.0 mol/L NaCl, R146 forms more favorable electrostatic interactions with D280, D315, and E430. However, R146 has unfavorable electrostatic interactions with K317, K338, and K340 of hIgG1. Thus, the free energy contribution of R146 is favorable by the sum of these interactions in 1.0 mol/L NaCl. Furthermore, the reinforced electrostatic interactions are beneficial to formation of the nonpolar interactions of N147 and I150 of helix II (Figure 4). Hence, addition of 1.0 mol/L NaCl is favorable for binding of helix II to hIgG1. Therefore, the compensation between helices I and II makes the total binding free energy almost unchanged.

2.0 mol/L NaCl. As shown in Figure 6, the contributions of all residues in helix II are very small, except E143. The 2.0 mol/L NaCl screens not only the intermolecular electrostatic interactions between helix II and hIgG1 but also the electrostatic solvation effect of helix II. Hence, helix II does not bind hIgG1 as tight as that in water (Figure 1). Thus, the hot spots of helix II lose their significant contributions in 2.0 mol/L NaCl (Figure 2). However, residues of helix I interact strongly with hIgG1 via the electrostatic interactions, especially for residues N130, Y133, and H137. The electrostatic interactions are beneficial to the affinity between helix I and hIgG1 in 2.0 mol/L NaCl (Figure 1). Besides, nonpolar interactions are also strengthened in 2.0 mol/L NaCl. For example, residues N130 and L136 of helix I have negative $\Delta\Delta G_{nonpolar}$. Hence, in 2.0 mol/L NaCl the contribution of helix II decreases, whereas the nonpolar and electrostatic interactions provided by helix I increase. The cancellation of the contributions between two helices makes the binding free energy insensitive to the high concentration of NaCl.

The effect of salt on the SpA−hIgG1 complex is different from that on some proteins, such as the Barnase−Barstar complex[54] and TBP−DNA complex.[58] Formation of these complexes is only driven by the electrostatic interactions. In addition, the intermolecular electrostatic interactions are favorable for these complexes, while the electrostatic solvation effects are unfavorable. The two types of electrostatic interactions are both screened in the salt solution. Hence, salt strengthens the affinity of the Barnase−Barstar complex, since the decrease of the intermolecular electrostatic interactions is smaller than that of the electrostatic solvation effect. In contrast, the decrease of the intermolecular electrostatic interactions of the TBP−DNA complex is greater than that of the electrostatic solvation effect, and thus, the affinity is weakened by salt. Therefore, for the complex driven by a single type of interaction, the binding free energy shows a trend of monotonic increasing or decreasing with the increasing ionic strength. However, there are nonpolar and electrostatic interactions between two helices of SpA and hIgG1. In addition, there exists the compensations between helices I and II of SpA as well as between the nonpolar and the electrostatic interactions. Thus, the affinity of the SpA−hIgG1 complex is independent of salt concentration, and the compensations are the basis of the salt tolerance of the SpA−hIgG1 complex.

3.2. Effect of pH on the Affinity of the SpA−hIgG1 Complex. The effect of pH on the affinity between SpA and hIgG1 is investigated by comparing the binding free energies at pH 3.0 and 7.0. At pH 7.0, SpA can bind hIgG1 stably and the binding free energy is −37.1 kcal/mol. At pH 3.0, however, the free energy is 11.9 kcal/mol (Table 3). It means that SpA cannot bind hIgG1 at pH 3.0. The calculated free energy is in line with the experimental observation that hIgG1 can be eluted effectively off the SpA affinity adsorbent at pH 3.0.[51] Figure 7 shows the values of F/R of SpA and hIgG1 at pH 3.0. The F/R value of SpA is higher than that of hIgG1 along the trajectory, and the average value of SpA along the last 10 ns trajectory is 0.82 (Figure 7). However, the F/R value of hIgG1 decreases from 1.0 to 0.6 gradually along the trajectory. It means that SpA always binds the

surface of hIgG1 during the simulation but slides slowly on the surface of hIgG1 and moves away from the consensus binding site of hIgG1. It is noted that although complete dissociation is not observed during the insufficient long trajectory (70 ns), it is predicted correctly by the free energy and the F/R data. Hence, the MD simulation here is also helpful to explore the dissociation mechanism of the SpA−hIgG1 complex at pH 3.0.

In order to identify the effect of pH on the contributions of interactions, the binding free energy was divided into the nonpolar and electrostatic interactions (Table 3). At pH 7.0, the nonpolar energy ($\Delta G_{nonpolar}$ = −59.8 kcal/mol) compensates for the positive electrostatic energy (ΔG_{PBelec} =22.7 kcal/mol) and the nonpolar term is the driving force of the binding. At pH 3.0, however, the positive electrostatic energy becomes larger (ΔG_{PBelec} =59.6 kcal/mol) and cannot be compensated for by the negative nonpolar energy ($\Delta G_{nonpolar}$ = −47.7 kcal/mol). Therefore, dissociation at pH 3.0 is mainly driven by the electrostatic interactions. In addition, the sources of the positive electrostatic energies are different at pH 7.0 and 3.0. It is known that the electrostatic energy (ΔG_{PBelec}) is the sum of the intermolecular electrostatic energy (ΔG_{elec}) and the electrostatic solvation effect (ΔG_{PB}) (eq 6). At pH 7.0, SpA and hIgG1 carry −2e and +3e charges, respectively. Thus, attractive intermolecular electrostatic interactions (−143.3 kcal/mol) exist between the oppositely charged residues, whereas the solvation energies of these charged residues are positive (166.0 kcal/mol), which are the source of the unfavorable electrostatic energy. At pH 3.0, however, SpA and hIgG1 carry +4e and +30e, respectively. Thus, all of the electrostatic residues are positively charged or neutral at pH 3.0. The intermolecular electrostatic energy (1497.6 kcal/mol) is unfavorable, while the solvation energy for protonation of the acidic residues (Glu and Asp) is favorable (−1438 kcal/mol) for binding. Finally, the intermolecular electrostatic repulsions, the source of the unfavorable electrostatic interactions, are the driving force of dissociation.

Figure 8 shows the comparison of the per-residue free energy contributions of SpA at pH 3.0 and 7.0. It is seen that the low pH dominantly affects the contributions of some hot spots (Y133, H137, E143, R146, and K154) and L136 of SpA. As the hot spots of helix II, R146 and K154 contribute the large unfavorable electrostatic energies for dissociation. At pH 7.0, R146 and K154 not only have repulsions with positively charged residues of hIgG1, such as R255, K288, K317, and K338, but also have the attractive interactions with negatively charged residues, including D249, E258, D280, D315, E333, E345, and E380 (Figure 9A). In addition, the total interactions of these residues are favorable for binding. When at pH 3.0, the negatively charged residues of hIgG1 turn neutral and their favorable interactions with R146 and K154 are missing (Figure 9B). However, the unfavorable interactions between the two residues (R146 and K154) and the positively charged residues of hIgG1 still exist. Thus, R146 and K154 contribute the large unfavorable electrostatic energies at pH 3.0. Another special residue of SpA is H137. H137 is neutral at pH 7.0 and has favorable interactions with the electrostatic residues of hIgG1, most of which are acidic residues. However, H137 is positively charged at pH 3.0 and has strong unfavorable interactions with the positively charged residues of hIgG1, such as H310, K317, H433, and H435. Thus, H137 provides the favorable energy for the association at pH 7.0 and the unfavorable electrostatic energy for the dissociation at pH 3.0. It is seen from Figure 9B that the unfavorable electrostatic interactions are dominantly provided by residues H137, R146, and K154 at

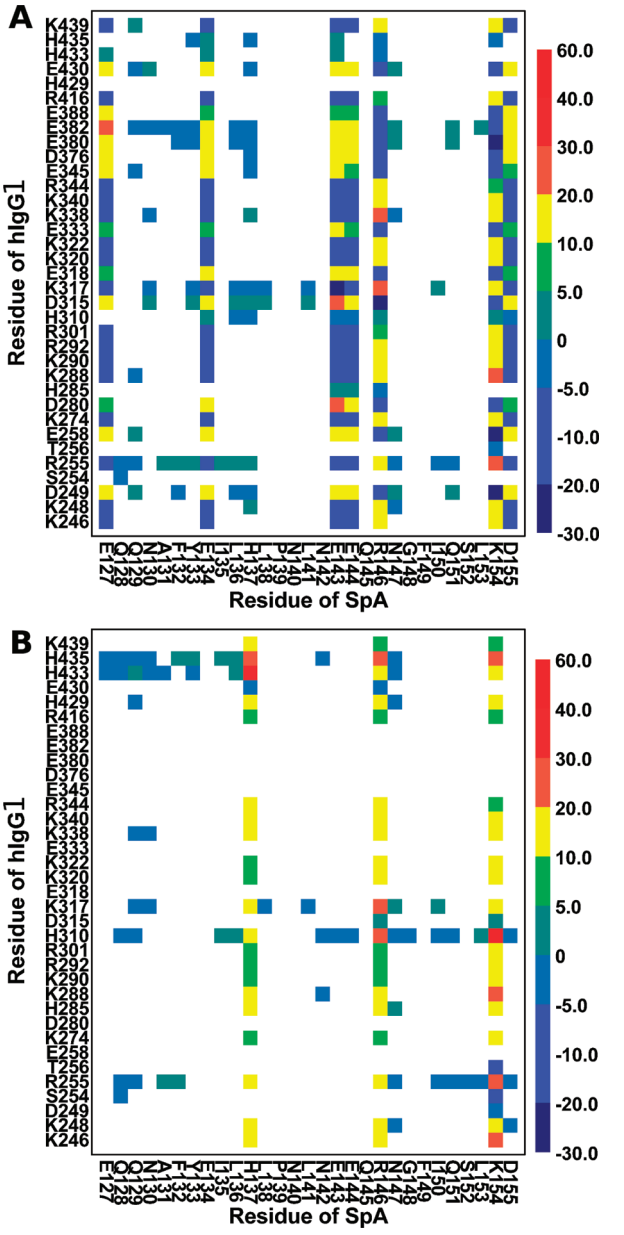

Figure 9. Pair interaction energy analysis between SpA and hIgG1 at pH 7.0 (A) and 3.0 (B). Figures are colored according to the interaction potential energy of each residue pair. Interaction energy ranges from blue (most negative) to red (most positive). Only the residues involving strong intermolecular interactions are displayed. The interactions with small potential energy ranging from −0.5 to 0.5 kcal/mol are not colored.

pH 3.0. Furthermore, the large unfavorable electrostatic interactions disrupt the nonpolar interactions between helix I and hIgG1. For example, the nonpolar contributions of Y133, L136, and H137 decreased significantly at pH 3.0 (Figure 8). The dissociation will take place until the nonpolar contribution decreases to zero in the case of the longer MD simulation. Hence, the electrostatic interactions provided by H137, R146, and K154 are the main driving force for dissociation of the SpA−hIgG1 complex at pH 3.0.

3.3. Refinement of the Binding Model of SpA. The molecular mechanism of the effects of salt and pH on the affinity between SpA and hIgG1 is applied to refine the simplified

dx.doi.org/10.1021/jp205770p |J. Phys. Chem. B 2012, 116, 424–433

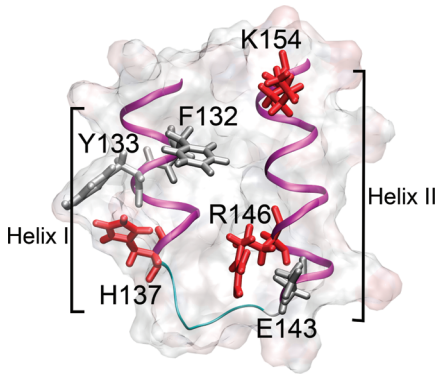

Figure 10. Simplified binding model of SpA. The hot spots are displayed by the licorice model. In addition, the first group contributing to association (F132, Y133, and E143) is colored in silver, while the second group contributing to dissociation (H137, R146, and K154) is in red. SpA is depicted by the surface and cartoon models. The surface is colored according to the charges of the atoms. Negatively and positively charged zones are depicted in red and blue, respectively.

binding model of SpA, which is built only based on the binding mechanism in our previous work.[17] In this model, six hot spots of SpA regulate the affinity of the complex. Herein, it is found that the affinity between SpA and hIgG1 is not affected by salt, although the salt affects the contributions of the hot spots of SpA. The salt tolerance of the affinity mainly originates from two aspects of compensation, with one between helices I and II and the other between the nonpolar and electrostatic interactions. Hence, all of the six hot spots of SpA should be considered in the model to ensure the salt-tolerance property of SpA. Furthermore, the hot spots can be divided into two groups. The first group contains F132, Y133, and E143, which always contributes significantly for the association. The second group contains H137, R146, and K154, which provides attractive interactions for the association at pH 7.0 and strong repulsions for the dissociation at pH 3.0. Thus, SpA seems like a ligand for hydrophobic charge induction chromatography. Therefore, to develop SpA-mimic ligands with high affinity and excellent salt tolerance, the molecular mechanisms of the association and dissociation should be considered in a rational design protocol. A more detailed model of SpA is constructed by coupling the molecular mechanism of dissociation, as shown in Figure 10. Since the hot spots in the model are located on the same side of the two helices, all Cα atoms of the hot spots lie in one plane. This is advantageous to the rational design of novel small-molecular or linear peptide ligands without considering the secondary structure, such as the helices of SpA. The model may be used as the starting point for rational design of novel SpA-mimic ligands of IgG.

4. CONCLUSIONS

MD simulations, MM/PBSA analysis, and free energy decomposition were adopted to study the salt and pH effects on the affinity interactions between SpA and hIgG1. It is confirmed that the total binding free energy is affected little by NaCl, but it is reduced greatly at pH 3.0. In other words, the adsorbed hIgG1 cannot be eluted off the SpA affinity adsorbent by NaCl but can be eluted effectively at pH 3.0. The results of free energy decomposition indicate that salt and pH mainly regulate the contributions of the hot spots of SpA (F132, Y133, H137, E143, R146, and K154) to affect the affinity between SpA and hIgG1. In salt solution, the intermolecular electrostatic interactions are favorable to the binding while the electrostatic solvation interactions are positive, which makes the total electrostatic interaction unfavorable. In addition, nonpolar interactions compensate for the unfavorable electrostatic interactions and become the driving force of the binding. Furthermore, the nonpolar and electrostatic interactions are affected by salt, resulting in the increase of the free energy contributions of some key residues and the decrease of some others located on helices I and II. Thus, the compensations between the two helices of SpA as well as between the nonpolar and electrostatic interactions make the binding free energy independent of the concentration of NaCl. On the contrary, the electrostatic solvation interactions are favorable to the binding at pH 3.0, while the intermolecular electrostatic interactions are unfavorable due to the strong electrostatic repulsions between residues H137, R146, and K154 of SpA and the positively charged residues of hIgG1. Thus, the strong electrostatic repulsions become the dominant force between SpA and hIgG1 and result in the dissociation at pH 3.0. The hot spots H137, R146, and K154 are the molecular basis of the dissociation. These findings about the dissociation mechanism are used to refine the binding model of SpA to hIgG1, which may be used as the starting point for rational design of high-affinity SpA-mimic ligands of IgG.

■ ASSOCIATED CONTENT

Supporting Information. Initial conformation of the SpA−hIgG1 complex, profiles of rmsd, and intermolecular potential energy for the SpA−hIgG1 complex in different solutions. This material is available free of charge via the Internet at http://pubs.acs.org.

■ AUTHOR INFORMATION

Corresponding Author

*Phone: +86 22 27404981 (Y.S.); +86 22 27406590 (F.-F.L.). Fax: +86 22 27406590 (Y.S.); +86 22 27406590 (F.-F.L.). E-mail: ysun@tju.edu.cn (Y.S.); fufengliu@tju.edu.cn (F.-F.L.).

■ ACKNOWLEDGMENT

This work was supported by the Natural Science Foundation of China (Grant Nos. 20636040, 20906068, and 20976126), the National Basic Research Program of China (973 Program, Grant No. 2009CB724705), and the Natural Science Foundation of Tianjin from Tianjin Municipal Science and Technology Commission (Contract No. 10JCYBJC04500).

■ REFERENCES

(1) Alkan, H.; Bereli, N.; Baysal, Z.; Denizli, A. *Biochem. Eng. J.* **2009**, *45*, 201–208.
(2) Persson, J.; Lester, P. *Biotechnol. Bioeng.* **2004**, *87*, 424–434.
(3) Ljunglöf, A.; Lacki, K.; Mueller, J.; C, *Biotechnol. Bioeng.* **2006**, *96*, 515–524.
(4) Azevedo, a.M.; Rosa, P.a.J.; Ferreira, I. F.; Aires-Barros, M. R. *J. Chromatogr. A* **2008**, *1213*, 154–161.
(5) Roque, A.C.a.; Silva, C. S. O.; Taipa, M. A. *J. Chromatogr. A* **2007**, *1160*, 44–55.
(6) Deisenhofer, J. *Biochemistry* **1981**, *20*, 2361–2370.
(7) DeLano, W. L. *Science* **2000**, *287*, 1279–1283.

(8) Li, R.; Dowd, V.; Stewart, D. J.; Burton, S. J.; Lowe, C. R. *Nat. Biotechnol.* **1998**, *16*, 190–195.
(9) Hale, G.; Drumm, A.; Harrison, P.; Phillips, J. *J. Immunol. Methods* **1994**, *171*, 15–21.
(10) Carter-Franklin, J. N.; Victa, C.; McDonald, P.; Fahrner, R. *J. Chromatogr. A* **2007**, *1163*, 105–111.
(11) Gouda, H.; Torigoe, H.; Saito, A.; Sato, M.; Arata, Y.; Shimada, I. *Biochemistry* **1992**, *31*, 9665–9672.
(12) Ljungberg, U. K.; Jansson, B.; Niss, U.; Nilsson, R.; Sandberg, B. E. B.; Nilsson, B.r. *Mol. Immunol.* **1993**, *30*, 1279–1285.
(13) Hahn, R.; Schlegel, R.; Jungbauer, A. *J. Chromatogr. B* **2003**, *790*, 35–51.
(14) Salvalaglio, M.; Zamolo, L.; Busini, V.; Moscatelli, D.; Cavallotti, C. *J. Chromatogr. A* **2009**, *1216*, 8678–8686.
(15) Moiani, D.; Salvalaglio, M.; Cavallotti, C.; Bujacz, A.; Redzynia, I.; Bujacz, G.; Dinon, F.; Pengo, P.; Fassina, G. *J. Phys.Chem. B* **2009**, *113*, 16268–16275.
(16) Boi, C.; Busini, V.; Salvalaglio, M.; Cavallotti, C.; Sarti, G. C. *J. Chromatogr. A* **2009**, *1216*, 8687–8696.
(17) Huang, B.; Liu, F. F.; Dong, X. Y.; Sun, Y. *J. Phys. Chem. B* **2011**, *115*, 4168–4176.
(18) Ehrlich, G. K.; Bailon, P. *J. Mol. Recognit.* **1998**, *11*, 121–125.
(19) McCue, J. T.; Kemp, G.; Low, D.; Quiñones-García, I. *J. Chromatogr. A* **2003**, *989*, 139-–153.
(20) Hober, S.; Nord, K.; Linhult, M. *J. Chromatogr. B* **2007**, *848*, 40–47.
(21) Smith, L. J.; Dobson, C. M.; van Gunsteren, W. F. *Proteins* **1999**, *36*, 77–86.
(22) Gattin, Z.; van Gunsteren, W. F. *ChemBioChem* **2008**, *9*, 923–933.
(23) Phillips, J. C.; Braun, R.; Wang, W.; Gumbart, J.; Tajkhorshid, E.; Villa, E.; Chipot, C.; Skeel, R. D.; Kalé, L.; Schulten, K. *J. Comput. Chem.* **2005**, *26*, 1781–1802.
(24) MacKerell Jr., A. D.; Brooks, B.; Brooks III, C. L.; Nilsson, L.; Roux, B.; Won, Y.; Karplus, M. CHARMM: The Energy Function and Its Parameterization with an Overview of the Program. In *Encyclopedia of Computational Chemistry*; Schleyer, P. v. R., et al. ; John Wiley & Sons: Chichester. 1998; Vol. 1, pp 271−277.
(25) Paterlini, M. G.; Ferguson, D. M. *Chem. Phys.* **1998**, *236*, 243–252.
(26) Feller, S. E.; Zhang, Y.; Pastor, R. W.; Brooks, B. R. *J. Chem. Phys.* **1995**, *103*, 4613–4621.
(27) Essmann, U.; Perera, L.; Berkowitz, M. L.; Darden, T.; Lee, H.; Pedersen, L. G. *J. Chem. Phys.* **1995**, *103*, 8577–8577.
(28) Ryckaert, J.; Ciccotti, G.; Berendsen, H. *J. Comput. Phys.* **1977**, *23*, 327–341.
(29) Srinivasan, J.; Cheatham, T. E.; Cieplak, P.; Kollman, P. A.; Case, D. A. *J. Am. Chem. Soc.* **1998**, *120*, 9401–9409.
(30) Massova, I.; Kollman, P. A. *J. Am. Chem. Soc.* **1999**, *121*, 8133–8143.
(31) Brooks, B. R.; Bruccoleri, R. E.; Olafson, B. D.; States, D. J.; Swaminathan, S.; Karplus, M. *J. Comput. Chem.* **1983**, *4*, 187–217.
(32) Zoete, V.; Meuwly, M.; Karplus, M. *Proteins* **2005**, *61*, 79–93.
(33) Friedman, R. A.; Honig, B. *Biophys. J.* **1995**, *69*, 1528–1535.
(34) Yan, C.; Kaoud, T.; Lee, S.; Dalby, K. N.; Ren, P. *J. Phys. Chem. B* **2011**, *115*, 1491–1502.
(35) Froloff, N.; Windemuth, A.; Honig, B. *Protein Sci.* **1997**, *6*, 1293–1301.
(36) Sheinerman, F. *J. Mol. Biol.* **2002**, *318*, 161–177.
(37) Liang, S.; Li, L.; Hsu, W. L.; Pilcher, M. N.; Uversky, V.; Zhou, Y.; Dunker, A. K.; Meroueh, S. O. *Biochemistry* **2009**, *48*, 399–414.
(38) Li, L.; Liang, S.; Pilcher, M. M.; Meroueh, S. O. *Protein Eng. Des. Sel* **2009**, *22*, 575–586.
(39) Moreira, I. S.; Fernandes, P. A.; Ramos, M. J. *Int. J. Quantum Chem.* **2007**, *107*, 299–310.
(40) Lafont, V.; Schaefer, M.; Stote, R. H.; Altschuh, D.; Dejaegere, A. *Proteins: Struct. Funct. Bioinform.* **2007**, *67*, 418–434.
(41) Méndez, R.; Leplae, R.; De Maria, L.; Wodak, S. J. *Proteins: Struct. Funct. Bioinform.* **2003**, *52*, 51–67.
(42) Zuo, Z.; Gandhi, N. S.; Mancera, R. L. *J. Chem. Inf. Model* **2010**, *50*, 2201–2212.
(43) Kollman, P. A.; Massova, I.; Reyes, C.; Kuhn, B.; Huo, S.; Chong, L.; Lee, M.; Lee, T.; Duan, Y.; Wang, W.; et al. *Acc. Chem. Res.* **2000**, *33*, 889–897.
(44) Yang, Y.; Qin, J.; Liu, H.; Yao, X. *J. Chem. Inf. Model* **2011**, *51*, 680–692.
(45) Ryde, U.; Weis, A.; Katebzadeh, K.; Soderhjelm, P.; Nilsson, I. *J. Med. Chem.* **2006**, *49*, 6596–6606.
(46) Massova, I.; Kollman, P. *Perspect. Drug Discovery Des.* **2000**, *18*, 113–135.
(47) Joshi, M.; Ebalunode, J. O.; Briggs, J. M. *Proteins* **2009**, *75*, 323–335.
(48) Liu, F. F.; Dong, X. Y.; He, L.; Middelberg, A. P.; Sun, Y. *J. Phys. Chem. B* **2011**, *115*, 11879–11887.
(49) Muzzioli, E.; Del Rio, A.; Rastelli, G. *Chem. Biol. Drug Des.* **2011**, *78*, 252–259.
(50) Hou, T.; Wang, J.; Li, Y.; Wang, W. *J. Comput. Chem.* **2011**, *32*, 866–877.
(51) Bottomley, S. P.; Sutton, B. J.; Gore, M. G. *J. Immunol. Methods* **1995**, *182*, 185–192.
(52) van Asselt, E. J.; Dijkstra, B. W. *FEBS Lett.* **1999**, *458*, 429–435.
(53) Goedken, E. R.; Marqusee, S. *J. Biol. Chem.* **2001**, *276*, 7266–7271.
(54) Bertonati, C.; Honig, B.; Alexov, E. *Biophys. J.* **2007**, *92*, 1891–1899.
(55) Baldwin, R. L. *Biophys. J.* **1996**, *71*, 2056–2063.
(56) Record, M. T., Jr.; Zhang, W.; Anderson, C. F. *Adv. Protein Chem.* **1998**, *51*, 281–353.
(57) Dominy, B. N.; Perl, D.; Schmid, F. X.; Brooks, C. L. *J. Mol. Biol.* **2002**, *319*, 541–554.
(58) Bredenberg, J. H.; Russo, C.; Fenley, M. O. *Biophys. J.* **2008**, *94*, 4634–4645.